International Journal of Mining, Reclamation and Environment

ISSN: (Print) (Online) Journal homepage: www.tandfonline.com/journals/nsme20

Optimal mine pitwall profiles in jointed anisotropic rock masses

Andrea Agosti, Scott D. Cylwik & Stefano Utili

To cite this article: Andrea Agosti, Scott D. Cylwik & Stefano Utili (09 Sep 2024): Optimal mine pitwall profiles in jointed anisotropic rock masses, International Journal of Mining, Reclamation and Environment, DOI: 10.1080/17480930.2024.2387988

To link to this article: https://doi.org/10.1080/17480930.2024.2387988

Published online: 09 Sep 2024.

INTERNATIONAL JOURNAL OF MINING, RECLAMATION AND ENVIRONMENT
https://doi.org/10.1080/17480930.2024.2387988

Taylor & Francis
Taylor & Francis Group

OPEN ACCESS Check for updates

Optimal mine pitwall profiles in jointed anisotropic rock masses

Andrea Agosti[a], Scott D. Cylwik[b] and Stefano Utili[a,c]

[a]OptimalSlope Ltd, Harwell Campus for Innovation and Science, London, UK; [b]Call & Nicholas, Inc, Tucson, AZ, USA; [c]School of Engineering, Newcastle University, Newcastle upon Tyne, UK

ABSTRACT

A new methodology based on the limit analysis upper bound method for the topological optimisation of slopes is presented, to determine geotechnically optimal slope profiles in anisotropic jointed rock masses. The methodology accounts for the effects of discontinuities such as joints, bedding planes, and tension cracks. We applied this methodology to the context of open pit mines, with the goal of achieving geotechnically optimal pitwall profiles. The optimal profiles maximise the Overall Slope Angle (OSA) while maintaining a prescribed Factor of Safety (FoS) and satisfying the geometric constraints imposed by benches and ramps. The method, implemented in the software OptimalSlope, utilises direction-dependent cohesion and internal friction angle parameters to replicate the effect of joints on slope stability. Key inputs include joint orientation, non-persistence, and probability of occurrence. We tested the methodology on a Mexican open pit mine to be excavated into Cretaceous siltstone featuring eight different joint sets and a primary bedding plane. Optimal pitwall profiles were determined for various combinations of bedding dip angles (0°, 15°, 30°, 45°, 60°, 75°, 90°) and mine pitwall orientations (hanging wall, footwall, side walls), considering the three-dimensional kinematics of the joints through anisotropic functions of cohesion and friction angle. Results indicate that the optimal pitwall profiles generally exhibit higher OSA compared to planar profiles with the same FoS, except in one bedding dip direction. Additionally, stability analyses performed using Rocscience Slide2 independently verified the FoS values of the optimal profiles.

ARTICLE HISTORY
Received 10 March 2024
Accepted 29 July 2024

KEYWORDS
Slope optimisation; mine pitwall design; slope stability; rock anisotropy; discontinuities; joints

1. Introduction

In the last four decades, a clear trend of open pit mines being excavated at increasing depths has emerged in the worldwide mining industry (Figure 1a). As existing mines deepen due to increased efficiency of mining equipment and improved exploration techniques, shallow ore bodies to be exploited have been progressively exhausted (Figure 1b). Between 1930 and 2000, the depth of the average discovery in Australia, Canada, and the United States increased from surface outcropping to 295 m [1]. Consequently, excavating pitwalls as steep as possible while maintaining geotechnical stability has grown in importance [2].

Anecdotal evidence that non-linear slope profiles in cross-section (*i.e*., a profile whose inclination varies with depth) are more stable than linear ones was first reported as far back as 1890 [4]. Newman observed that cuttings of concave shape excavated in homogeneous clay layers tended to be more stable than planar ones with the same OSA, which are more stable than cuttings of convex shape. Almost a century later, Hoek & Bray [5], analysed the stability of some concave circular

CONTACT Stefano Utili stefano.utili@newcastle.ac.uk School of Engineering, Newcastle University, Newcastle Upon Tyne, UK

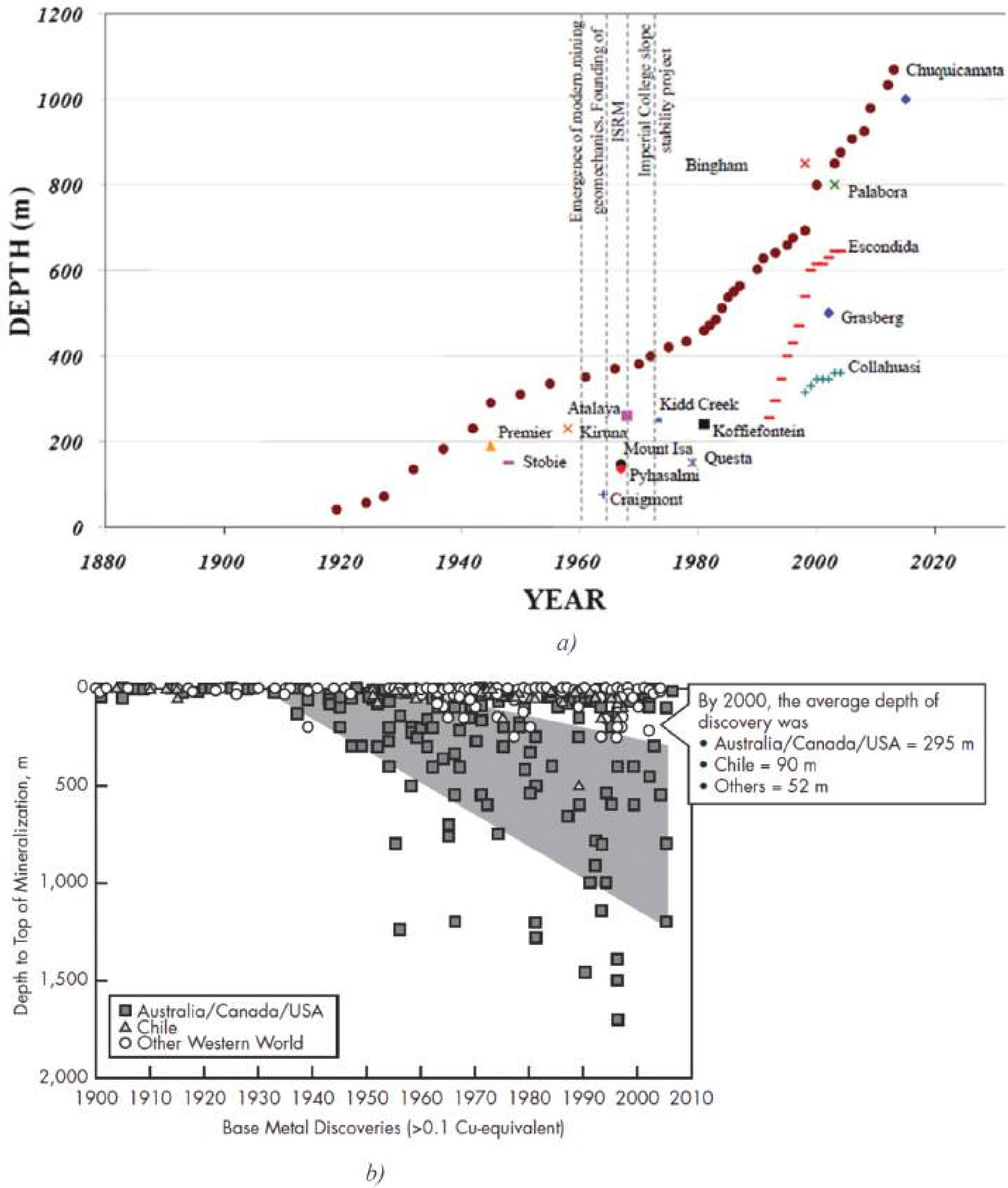

Figure 1. a) increasing depth of open pit mines over the years, after [3]; b) average depth of newly discovered ore deposits, after [1].

slopes in cross-section and found that the FoS for circular profiles was higher than for their planar counterparts (i.e. the planar slopes with the same OSA) which share the same toe and crest points. The first systematic theoretical study on the mechanical properties of concave uniform slope profiles for geomaterials exhibiting some cohesion, applicable to all rocks and clayey soils, appeared in Utili and Nova [6]. They proved that log spiral profiles exhibit higher FoS than their planar counterparts for any considered value of cohesion (c) and internal friction angle (φ). Later, other researchers [7–9] independently reached the same conclusion concerning the superior stability of non-linear (concave) uniform slope profiles albeit using different methods for assessing slope stability, such as the slip line method, limit equilibrium methods (LEM), and the finite element method.

A fundamental limitation of these studies is the assumption that the optimal shape is found as that associated with the highest FoS among curves belonging to a very restricted family, and the assumption of uniform slope. Recently, a new geotechnical software, OptimalSlope [10], was introduced to calculate the optimal slope profile for any specified lithological sequence without restricting the search to any predefined family of shapes. To quantify the gains of Net Present Value (NPV) and carbon footprint reduction consistently, in Agosti et al. [11,12], Utili et al. [13], and Agosti et al. [14] two independent designs of the open pit mines considered were performed: one with planar pitwalls and the other one with optimally shaped pitwalls exhibiting the same Factor of Safety as the planar ones. Financial and environmental gains were calculated as the difference in NPV, carbon footprint, and energy consumptions between the two designs, achieving cost reductions ranging from 12 to 140 million USD and carbon footprint reductions of 600,000 tonnes CO_2 on average per mine.

A fundamental limitation in the aforementioned works is the assumption of isotropic rock mass strength. However, accounting for the directional dependence of rock strength is increasingly required in the open pit mining industry, as evidenced by the growing number of publications dedicated to rock mass strength anisotropy in key geotechnical and mining journals and conferences (e.g [15–25]), LOP guidelines [26,27], and the availability of general anisotropic shear strength models in mainstream geotechnical software packages such as Rocscience Slide2 and RS2.

In this paper, the methodology presented in Utili et al. [13] for the topological optimisation of isotropic slope profiles is extended for the first time to rock masses of anisotropic shear strength in order to account for the effect of joint-sets, tension cracks and anisotropic intact rock. Since most rock masses encountered in open pit mines feature several joint sets and often anisotropic intact rock, this development is crucial to extend the applicability of pitwall optimisation to all open pit mines.

The paper is structured as follows: Section 2 reviews the main modelling techniques in the literature for anisotropic shear strength of rock masses. Section 3 introduces the new algorithm for the determination of optimal slope profiles accounting for rock mass anisotropic strength. Section 4 presents a case study of a mine excavated in a typical bedded sedimentary rock mass and determines the anisotropic shear strength parameters based on the methodology recently introduced by Cylwik [28] to determine equivalent anisotropic (c, φ) parameters for jointed rock masses. Section 5 illustrates the optimal profiles determined for several scenarios of pit excavation. Section 6 provides a discussion of the results achieved. Finally, Section 7 presents the conclusions.

2. Modelling anisotropic rock mass shear strength

2.1. Main modelling technique

In the literature, the methods to describe anisotropic rock mass strength can be classified into two main approaches: a discrete (or discontinuum) approach and an equivalent continuum approach. For discontinuum modelling, various techniques are available to explicitly simulate the presence of joints and anisotropic rock mass. For example, in the framework of discrete-element modelling, the so-called synthetic rock mass model allows for the detailed consideration of the rock mass joint fabric to determine rock mass strength at large scales [22,29]. Although this model has great promise for the future of rock slope stability modelling [27], the current computational power and data requirements make it impractical for the design and assessment of the stability of pitwalls [23].

FLAC3D, a commercial finite difference code, includes the ubiquitous-joint model to account for anisotropy induced by planes of weakness and beddings [30,31]. In such cases, a direction dependent Mohr–Coulomb strength criterion with tension cut-off, which assumes lower strength in the direction of a single structure without explicitly modelling any rock joints is used. However, this approach is not suitable for capturing the anisotropic strength of a rock mass featuring several joint sets since many different planes of weakness would have to be considered concurrently and their shear strength calibrated from the joint dataset, for which a methodology is not yet available.

In this paper, an equivalent continuum approach to model rock mass anisotropy (i.e. the use of equivalent shear strength parameters) is employed. The Mohr–Coulomb (M-C) criterion has been extended to account for anisotropic behaviour of soils since Lo [32]. Significant work has also been performed by Chen [33] using the limit analysis upper bound method to investigate the stability of slopes in anisotropic soils, with the strength parameters c and φ assumed to vary with the loading direction according to sine and cosine functions. This work was recently extended to account for tension cracks by Stockton et al. [34] using the LEM.

However, it is now well established that the strength of rocks is better described by the Hoek-Brown (H-B) criterion rather than the M-C [27] and the type of directional dependency exhibited by soil shear strength cannot be assumed for rock. However, the H-B criterion [35] and its extension to rock masses, the Generalised Hoek-Brow (G-H-B) [36] were formulated only for isotropic rocks. Although significant work has been done to extend the G-H-B to anisotropic intact rock [37–39], the presence of discrete discontinuities such as bedding planes and joint sets are not currently captured by such extensions.

To capture the effect of joint sets and bedding planes on the rock mass strength, anisotropic strength models can be employed. Mercer [19] defines an anisotropic strength model as 'a constitutive model that describes the shear strength of an anisotropic rock mass in relation to the change in the angle between the plane of shear, and either the predominant plane of weakness of the rock fabric or the predominant orientation of major structural weakness'. Arguably, Jaeger's analytical solution can be considered such a model [40]. These models have become popular among slope stability practitioners over the last 15 years with the implementation in Rocscience Slide2 of five anisotropic material models [24].

One of the first models to gain popularity was the first-generation Snowden Anisotropic Linear Model (ALM) proposed by Snowden Mining Consultants in 2005. Subsequently, second (ALM2, see Figure 2) and third generation (ALM3) models were introduced [19–21]. These models were formulated and calibrated to capture the anisotropic behaviour of a specific rock formation: the banded ironstone formations (BIF) of the Pilbara region in Western Australia [41]. However due to lack of experimental data, the Snowden models have been often used to model strength anisotropy

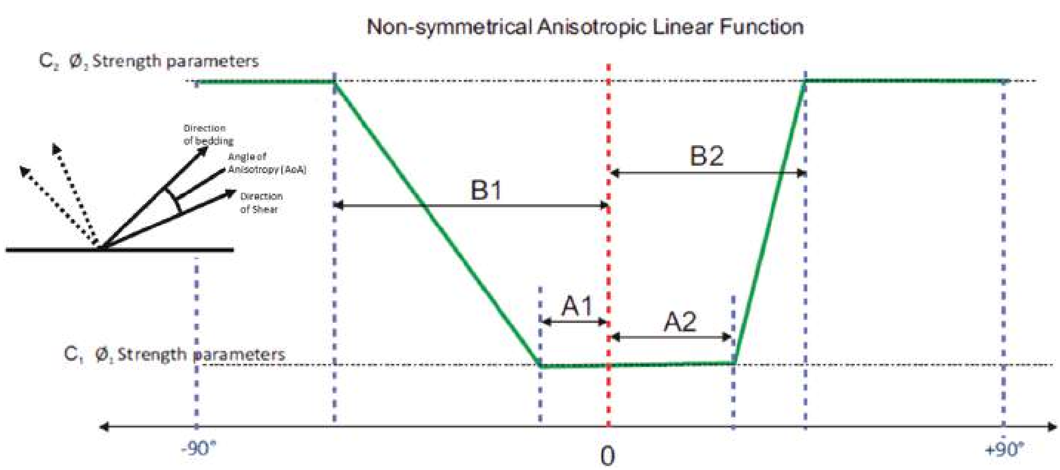

Figure 2. On the left, the definition of angle of anisotropy. On the right, the second generation of ALM strength criterion (redrawn after [36]). A1, A2, B1, and B2 are the model parameters.

of rock masses for mines excavated in different formations across the world. But since the Snowden parameters (A, B) were originally devised for and calibrated on the Pilbara BIF, a full re-calibration is required for them to be used on any rock formation other than the Pilbara BIF. Moreover, a linear model appears overly simple to capture the anisotropic shear strength of rock masses in sedimentary rocks, since they often exhibit several joint sets leading to a highly non-linear dependence of strength on shear direction.

2.2. Consideration of rock mass anisotropy in three dimensions

In 2005, Ryan proposed a method to determine equivalent anisotropic c and φ parameters for a rock mass characterised by a single joint-set in 2D, with the resulting c and φ parameters varying non-linearly with the direction of loading [42]. Recently, Cylwik has developed an extended methodology that estimates equivalent anisotropic (c, φ) parameters for rock masses with any number of joint sets in 3D, accounting for information on both orientation and persistence of the joint sets [28]. This anisotropic strength is estimated for any direction of shear (i.e. any cross-section orientation obtained by a plane cutting the 3D rock mass) based on intact rock strength, rock discontinuity set statistics, discontinuity strength, and Rock Quality Designation (RQD). The methodology is applicable to any type of co-planar discontinuities that may weaken the rock mass. It does not consider discrete block failure modes such as block toppling, and therefore these types of failure mechanisms must be considered separately.

This method provides reduced strength for shear in directions parallel to jointing and increased strength for shear in directions non-parallel to jointing, with a continuous function of strength in between the two extremes. Details on the methodology can be found in Cylwik [28] and are not repeated here.

A key observation is that the anisotropic model resulting from the determination of the equivalent c and φ parameters can be highly non-linear, with the anisotropic strength of the rock mass varying continuously with the direction of loading [28]. Therefore, it is important to input the c versus loading shear direction and φ versus loading shear direction functions correctly in any software employed for slope stability analysis.

3. New algorithm for topological optimisation of slopes excavated in jointed anisotropic rock masses

A detailed explanation of how slope profile optimisation works in case of slopes in non-jointed lithological units can be found in Utili et al. [13], therefore it will not be repeated here. The input data required are the rock mass strength (expressed as either Mohr-Coulomb or Generalised Hoek-Brown criterion), unit weight, and the geometries of benches (bench height and face inclination) and ramps and any overburden, if present. In Figure 3, typical input and output data are reported.

Here we present the new algorithm designed to determine optimal slope shapes in the presence of any number of discontinuities and of anisotropic intact rock.

3.1. Optimal slope profiles for anisotropic rock masses

For homogeneous slopes characterised by anisotropic rock strength, the optimal profile shape is determined by the main algorithm based on a prescribed input OSA. The optimal profile is associated with the largest stability factor, a dimensionless single scalar parameter which was initially introduced by Taylor [43] for developing dimensionless stability charts. This factor remains widely used for comparing the performance of different slopes. For an anisotropic M-C geomaterial, we define the stability factor as:

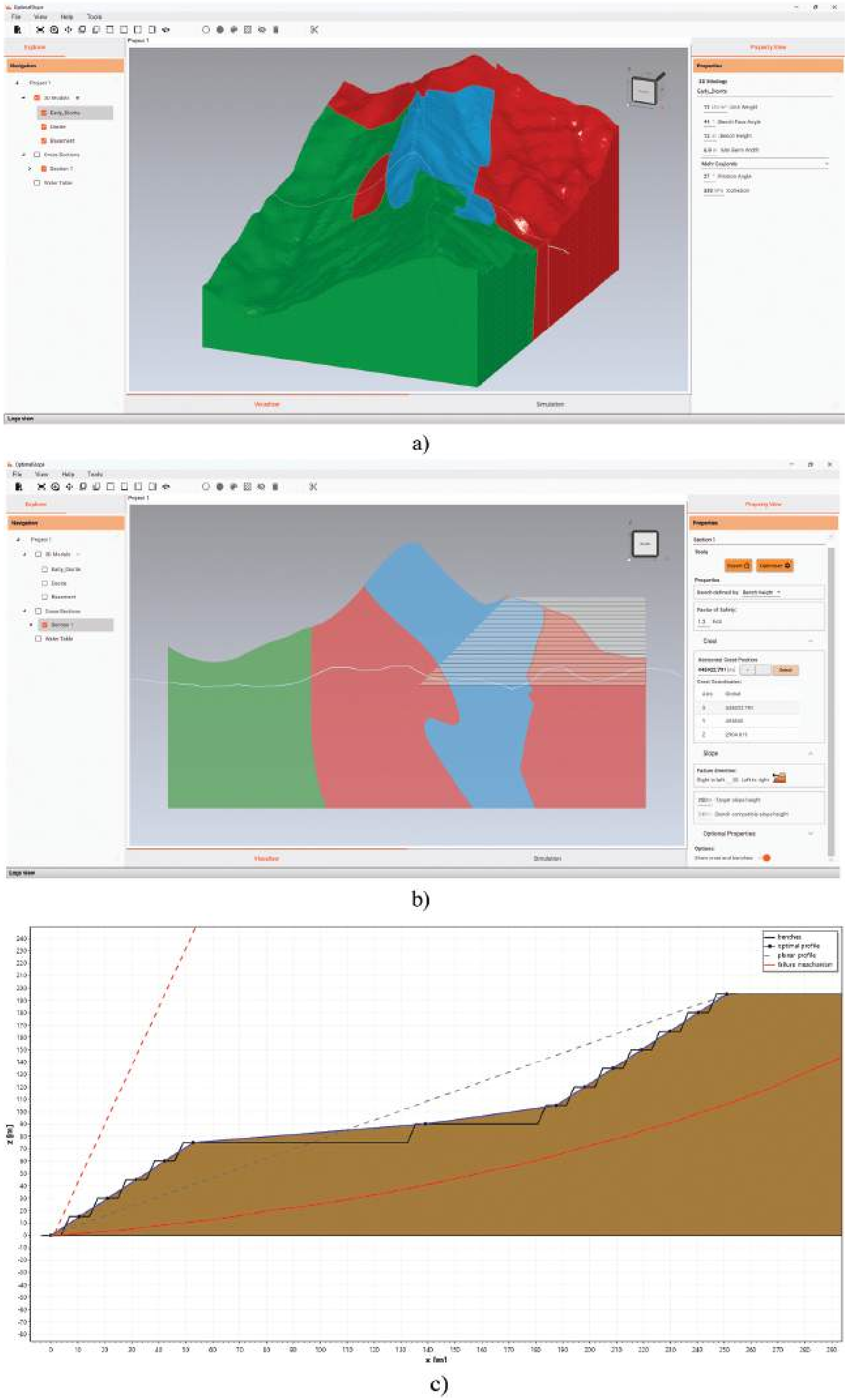

Figure 3. a) OptimalSlope graphical user interface showing a 3D input stratigraphy. For each lithological unit, rock strength parameters (c and φ for Mohr-Coulomb or GSI, UCS and m_i for G-H-B) are specified together with unit weight. Bench and ramp geometries are specified also for each lithological unit; b) vertical cross sections are sliced corresponding to the critical/

$$N_s = \frac{\gamma \cdot H}{c_{rm}} \tag{1}$$

where γ is the rock unit weight, H is the slope height, and c_{rm} is the equivalent cohesion for the rock mass yet to be determined. The slope profile with the largest stability factor also exhibits the largest FoS.

The main slope optimiser algorithm computes the stability factor using the upper bound theorem of limit analysis. The theorem states that a slope will collapse under its own weight if, for any assumed kinematically admissible failure mechanism, the rate of external work done by the soil weight exceeds the rate of internal energy dissipation [33]. Chen [33] tackled anisotropic slopes assuming only cohesion to be anisotropic with the internal friction angle assumed isotropic instead. This leads to unrealistically low FoS estimates for the slope due to a too conservative transition between rock mass strength and bedding strength [19]. In contrast, our new algorithm assumes both cohesion and internal friction angle as anisotropic.

For any potential failure mechanism (Figure 4a), the external and dissipated work expressions must be calculated [13]. The potential failure surface is now divided into piecewise segments, each with an average inclination ($\alpha_{fail,i}$). This inclination, along with the relationships between (c, φ) and the apparent dip of the failure surface (see Section 2), is here used to calculate the differential shear strength and corresponding c_i and φ_i values (Figure 4b). These values are then used to compute the rate of dissipated energy and external work.

The expression of the rate of dissipated energy is:

$$\dot{W}_D = \sum_i \int_{\theta_{i-1}}^{\theta_i} c_i \cdot \left(V \cdot \cos\varphi_i\right) \cdot \frac{r}{cos\varphi_i} \cdot d\theta = \sum_i c_i \cdot r_0^2 \cdot \Omega \cdot \int_{\theta_{i-1}}^{\theta_i} e^{2 \cdot \tan\varphi_i \cdot (\theta_i - \theta_0)} \cdot d\theta \tag{2}$$

where θ and r are the polar coordinates of the piecewise segment of the failure surface, r_0 the length of the chord OB (Figure 4a), and V and Ω are the tangential and angular velocity respectively of the failing rock mass ABC (Figure 4a).

The rate of external work is:

$$\dot{W}_E = \gamma \cdot r_0^3 \cdot f_{fail}\left(\theta_0, \theta_h, \varphi_{eq}, H\right) \tag{3}$$

where $f_{fail}\left(\theta_0, \theta_h, \varphi_{eq}, H\right)$ is a function of the geometry of the considered failure mechanism, and φ_{eq} is the equivalent internal friction angle used heuristically to account for the relationship between φ and apparent dip of the failure surface.

The stability factor (N_s) is derived for any potential failure mechanism considered by equating the rate of dissipated energy with the rate of external work. For each given slope profile, its failure mechanism is determined among all the potential failure mechanisms considered, as the one associated to the lowest stability factor (hence to the lowest FoS). Note that given the non-planar slope profile shape and anisotropic rock strength, the failure mechanism could also daylight anywhere above the slope toe. Therefore stability calculations are repeated for all the segments of the slope profile (a segment of slope profile is any part of the slope with a bottom point above the toe and/or a top point below the crest) to account for any local failure mechanism with entry and exit points located between slope toe and crest. Additionally, any water table and phreatic load effects can be easily included in limit analysis, as shown by Michalowski [44].

representative cross section for each mine sector; c) the output optimal profile obtained for a vertical cross section: benches and ramps are indicated by the black line whilst the blue line connects the midbench points representing the idealised profile that is passed as input to the block model for strategic mine planning (e.g. to software packages such as Geovia Whittle, Hexagon MinePlan, datamine NPVS).

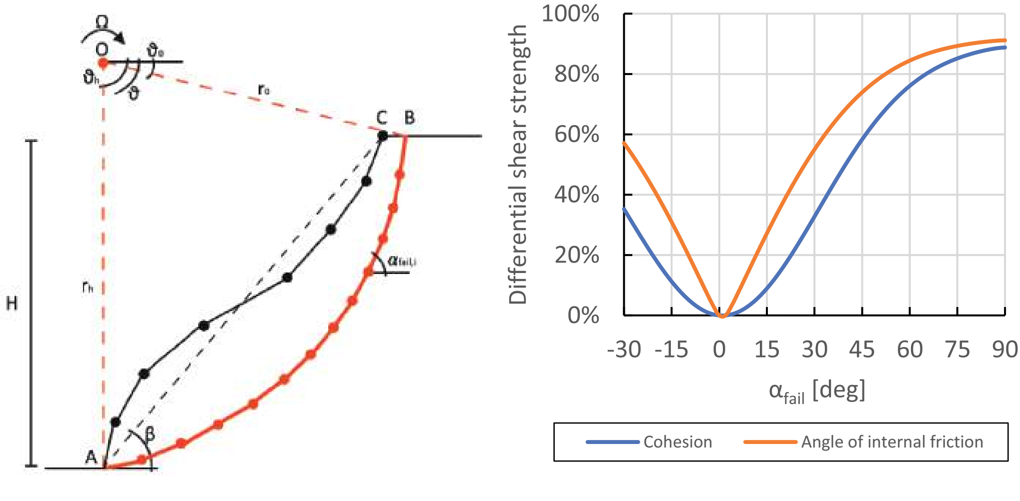

a) *b)*

Figure 4. (a) optimal slope profile with candidate failure surface. b) relationships between the differential shear strength and dip of the failure surface α_{fail}.

The dip of the failure surface versus *c* and dip of the failure surface versus φ functions are provided in discretised form as a series of points. To obtain a result independent of the choice of discretisation, a discretisation interval no larger than 1 degree was employed.

Note that the methodology proposed is valid for any anisotropy function. While linear normal stress – shear strength functions were employed, non-linear functions such as Barton-Bandis for bedding strength can also be implemented once linearised.

3.2. Consideration of tension cracks

The Cretaceous aged siltstone of the mine case study here considered (see Section 4) is subject to tension cracks. The formulation to account for tension cracks of any depth and at any locations in a slope in the framework of limit analysis is provided by Utili [45].

Note that in OptimalSlope slope optimiser the tension crack depth is an input. The program determines the optimal slope profile for a specified tension crack depth and anisotropic rock mass strength. Hence if the user is confident about the extent of the tension crack depth (e.g. from measurements or experience or stress analysis), no iterations are required.

Nevertheless in the mine case study here considered, the depth of tension crack was not known, hence we decided to opt for the most conservative of the approaches i.e. to assume the crack depth most adverse to the stability of the pitwall as detailed in [45]. The flow chart in Figure 5 outlines the procedure we employed. Initially, the optimal slope profile is computed by OptimalSlope without any tension cracks, i.e. assuming the slope to be intact. Then we performed a LEM analysis of the determined profile in Slide 2. The position of the line of thrust of the critical failure mechanism identified by Slide2 is checked relative to the failing mass. If parts of the line of thrust lie outside the failing mass, indicating slices in tension, a parametric analysis with increasing tension crack depths is performed in Slide2 to identify the most adverse tension crack. Typically the slope FoS decreases monotonically with increasing tension crack depth until a minimum value is reached (see Figure 6) which provides the most adverse tension crack for the slope, in terms of both depth and location. If the resulting slope FoS is lower than the target FoS (FoS_{target}) of more than 1%, OptimalSlope slope optimiser is run again assuming the tension crack depth determined for the previous optimal profile (previous iteration) as input. The iterative procedure continues until an optimal slope profile is found such that it satisfies the acceptability criterion

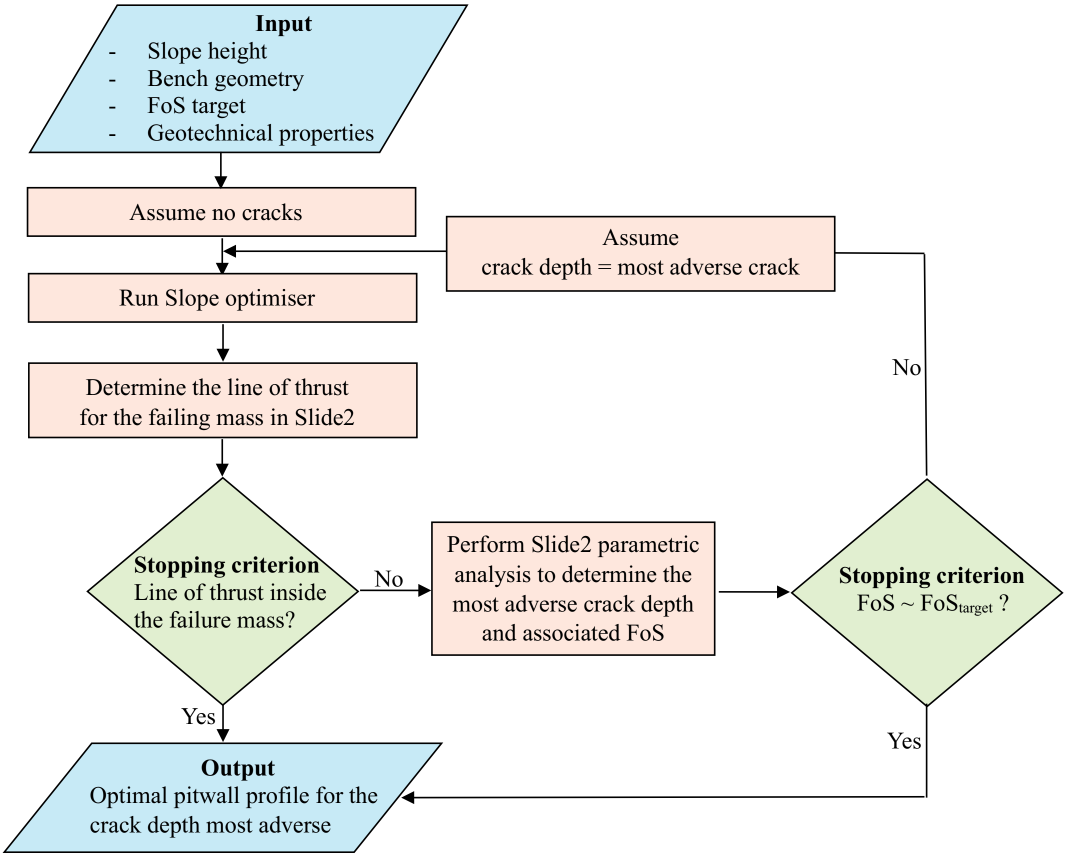

Figure 5. Procedure employed to account for tension cracks in determining optimal slope profiles.

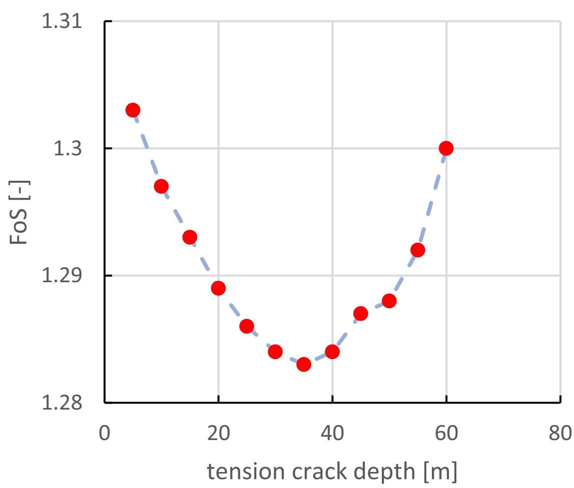

Figure 6. Typical result of a parametric slope stability analysis for various tension crack depths.

(slope FoS within 1% from the FoS_{target}) and the line of thrust of its failure mechanism is entirely inside the failing mass.

In Slide2, the anisotropic function is specified as a series of discretized points, necessitating a discretisation interval no larger than 1 degree for the dip of the failure surface versus c and φ functions to ensure result independence from discretisation choice.

4. Case study

The rock mass considered for this study is a Cretaceous-age siltstone where an open pit mine in central Mexico is excavated. The siltstone exhibits predominant bedding and crossbedding, which is variable in orientation due to gentle undulating folds across the property. A photograph of the rock mass is shown in Figure 7.

Figure 7. Photograph of the siltstone of the mine case study considered.

4.1. Structural data

The cell mapping technique was used to collect joint set orientation, length, and spacing data [42,46]. A negative exponential distribution is used to model both joint spacing and length. To combine mapping cells from across the site, the structural data from each group of cells was rotated so that the mean vector of the bedding set is flat (dip and dip direction of zero degrees). The structural dataset, rotated so that the flat bedding orientation is at 0 degrees, is shown in the lower hemisphere stereonet in Figure 8.

4.2. Rock strength testing

Direct shear tests were performed on natural fractures from core drilling in the siltstone to determine mean values of the joint friction angle and cohesion. The shear stress/normal stress regression plot of 22 samples is shown in Figure 9, and results in a mean friction angle of 24.16 degrees. Uniaxial and triaxial compression testing was performed on 25 HQ3-size intact core samples (63.5 mm diameter) and resulted in a mean intact internal rock friction angle of 48.6 degrees and cohesion of 8,924 kPa, as shown in Figure 10. The measured density of the rock is 26.2 kN/m^3.

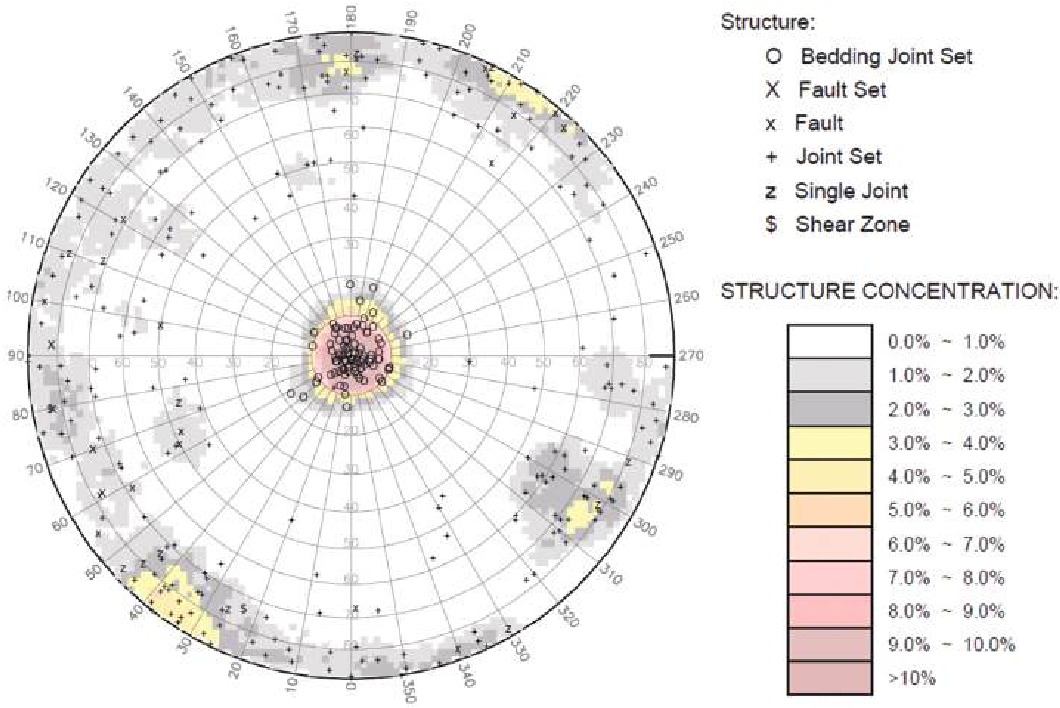

Figure 8. Lower hemisphere stereonet of siltstone structural data.

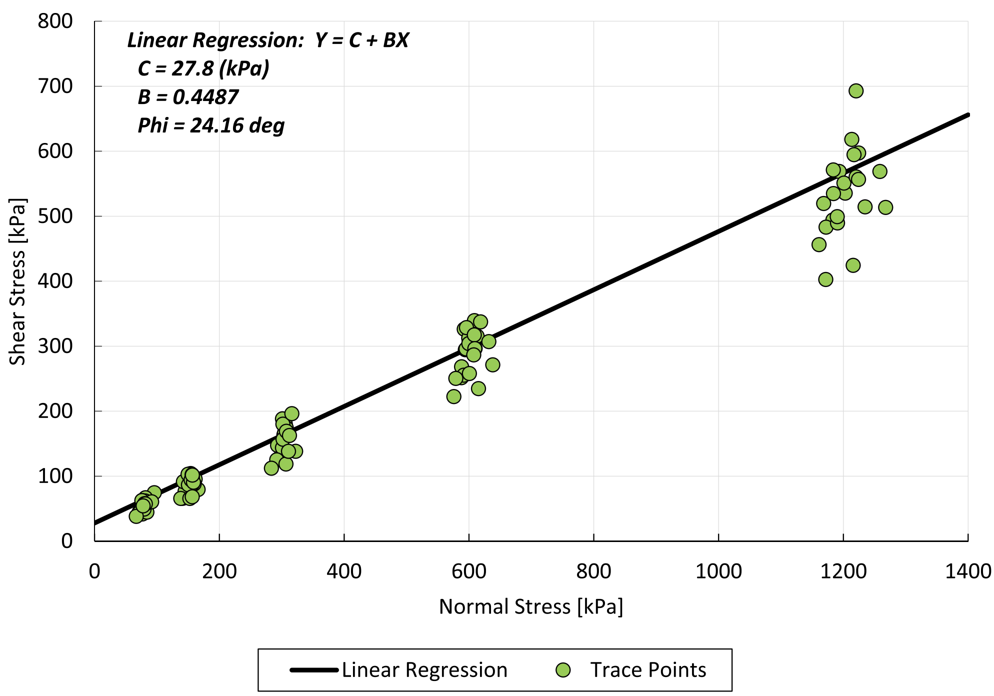

Figure 9. Shear stress vs. normal stress regression plot of 22 sample points. The data points are obtained from direct shear tests on natural fractures.

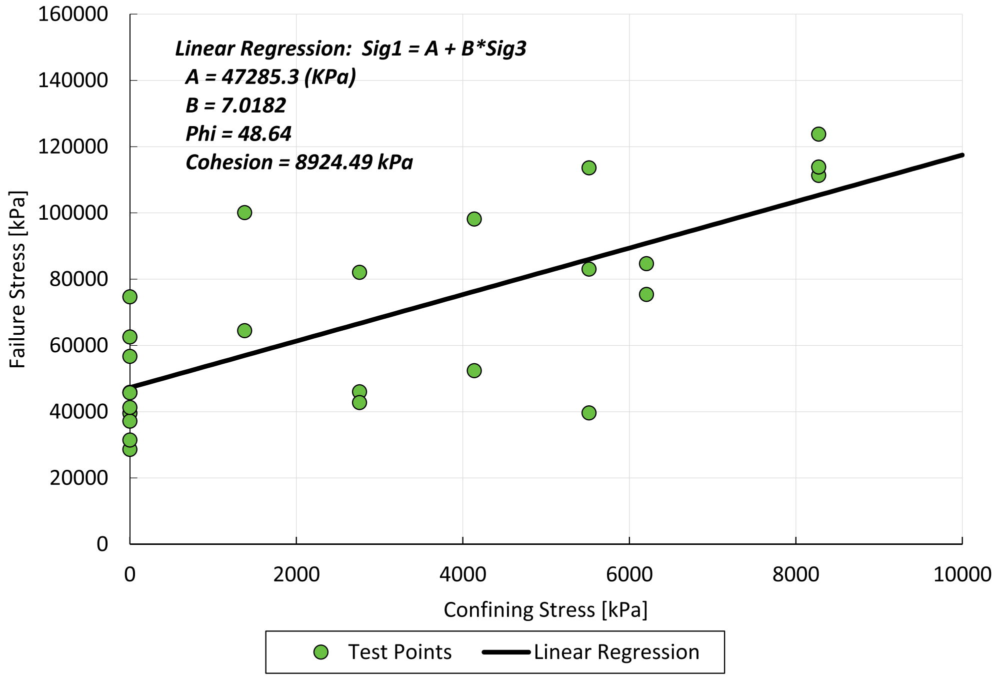

Figure 10. Uniaxial and triaxial compression tests plot of 25 sample points.

4.3. Anisotropic strength estimation

The anisotropic strength of the bedded siltstone was estimated using the freely downloadable calculation worksheet [47]. Example input parameters and estimated anisotropic strengths are shown in Figure 11 for a bedding dip of 60 degrees. Lower hemisphere stereonets show both the structure data and the estimated anisotropic cohesion. Charts of rock mass cohesion and friction angle are shown for cross-section azimuths of 0, 180, and 270 degrees. The azimuths of 0 and 180 degrees exhibit highly anisotropic behaviour versus dip angle, while the azimuth of 90/270 degrees exhibits nearly isotropic behaviour.

4.4. Joint dataset and cross-sections considered

To consider the effects of anisotropic rock mass strength on the geotechnically optimal slope profile, a sensitivity analysis was conducted by examining different inclinations of bedding within the siltstone. Dip values of 0, 15, 30, 45, 60, 75, and 90 degrees with the bedding dipping to the south were analysed by rotating the structural data in three dimensions. An example stereonet plot of bedding rotated to a dip of 45 degrees is shown in Figure 12.

Three different wall orientations in relation to the dip direction of bedding were considered for a total of 21 pitwall scenarios. The orientations are here termed as footwall, hanging wall, and end wall according to classical open pit terminology. Their definition is given as (see Figure 12):

- On the footwall, the bedding dips into the excavation (dip direction = 180°).
- On the hanging wall, the bedding dips back into the slope (dip direction = 0°).
- On the end walls, the bedding dips perpendicular to the slope (dip direction = 90° or 270°).

The siltstone rock mass utilised for this study is representative of many bedded ore deposits that contain well-defined bedding and cross bedding sets. The results of this sensitivity study are

Fracture Strength		
Cohesion	28	kPa
Phi	24.2	deg
Intact Rock Strength		
Cohesion	8,924	kPa
Phi	48.6	deg
	RQD:	**30%**

	Probability of Occurrence	Dip Direction (deg)	Dip (deg)	Mean Length (ft/m)	Mean Spacing (ft/m)	Strength Reduction Along Joints
Joint Set 1	1.00	180	60	15.8	0.2	0.00
Joint Set 2	0.44	109	89	10.1	1.4	0.57
Joint Set 3	0.33	342	43	6.1	1.3	0.69
Joint Set 4	0.26	46	52	7.5	1.3	0.75
Joint Set 5	0.42	264	63	7.0	1.4	0.60
Joint Set 6	0.19	337	26	7.7	1.6	0.82
Joint Set 7	0.37	65	39	7.1	1.3	0.65

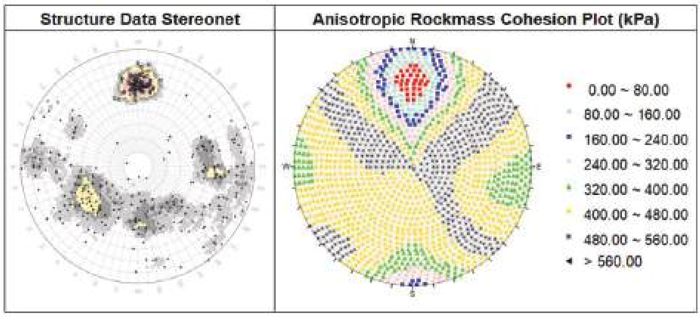

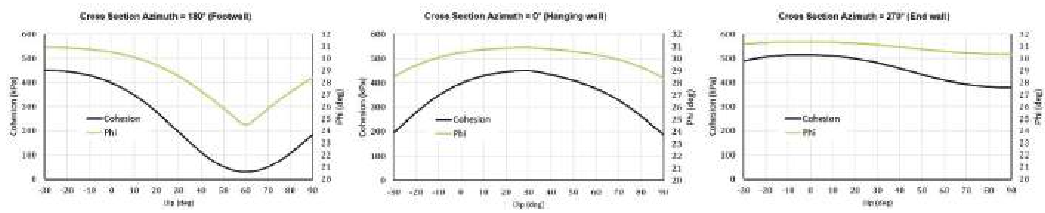

Figure 11. Calculation worksheet to calculate equivalent anisotropic (i.e. direction dependent) c and φ values versus the apparent dip of the shear plane for a bedding dip of 60 degrees to the south.

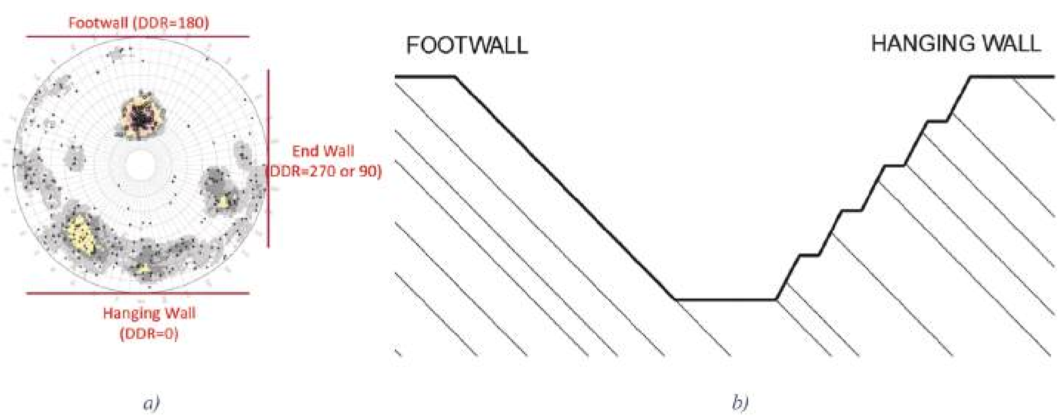

Figure 12. (a) example of stereonet of bedding rotated of 45 degrees with footwall, hanging wall, and end wall orientations shown. b) visualisation of footwall and hanging wall in the reference vertical cross section. The end wall lies in the out of plane direction.

relevant for numerous mining environments throughout the world, as many economic deposits are strata-bound and therefore the slopes exhibit footwall/hanging wall geometries.

The following parameters are assumed in the analysis:

- 195-metre-high slope with 15-metre-high benches
- Max interramp slope angle of 55 degrees (controlled by bench geometry parameters)
- Design acceptance criterion: FoS ≥ 1.30 for the overall slope scale and FoS ≥ 1.0 for the bench scale

5. Pitwall design

As per standard mining practice, benches are designed first, followed by the overall pitwall profiles [27,48]. We computed the minimum berm width, b_w, using the equation proposed by Hartman et al. [49] derived from the modified Ritchie's criteria, which has been demonstrated to be effective in field tests in several mines [50]:

$$b_w[m] = 4.5[m] + 0.2 \cdot H_{bench} \tag{4}$$

The maximum bench face angle was calculated equal to 70 degrees based on the capabilities of the rope shovel used to excavate the benches at the mine. The FoS was then verified by the Limit Equilibrium Method Morgenstern-Price [51], which is a rigorous LEM method where all equations of equilibrium are imposed on all slices using the Rocscience software Slide2 with non-circular failure surfaces and other default settings, including optimisation routines.

All analysed pitwall profiles are defined by a discrete set of points in the vertical plane: see the (x_i, z_i) coordinates in Figure 12, with z_i being values specified according to the bench height (Δz = bench height) input by the user, and x_i unknown variables to be determined [13]. The search for the optimal profile is constrained to feasible profiles (which lie within the blue bounds of Figure 13). A profile is feasible if $\frac{Z_i - Z_{i-1}}{x_i - x_{i-1}} \leq \tan \alpha_{imax}$ for every i (i.e. the inclination of each segment of the profile is capped to α_{imax}). The α_{imax} values are determined by the software before the optimisation

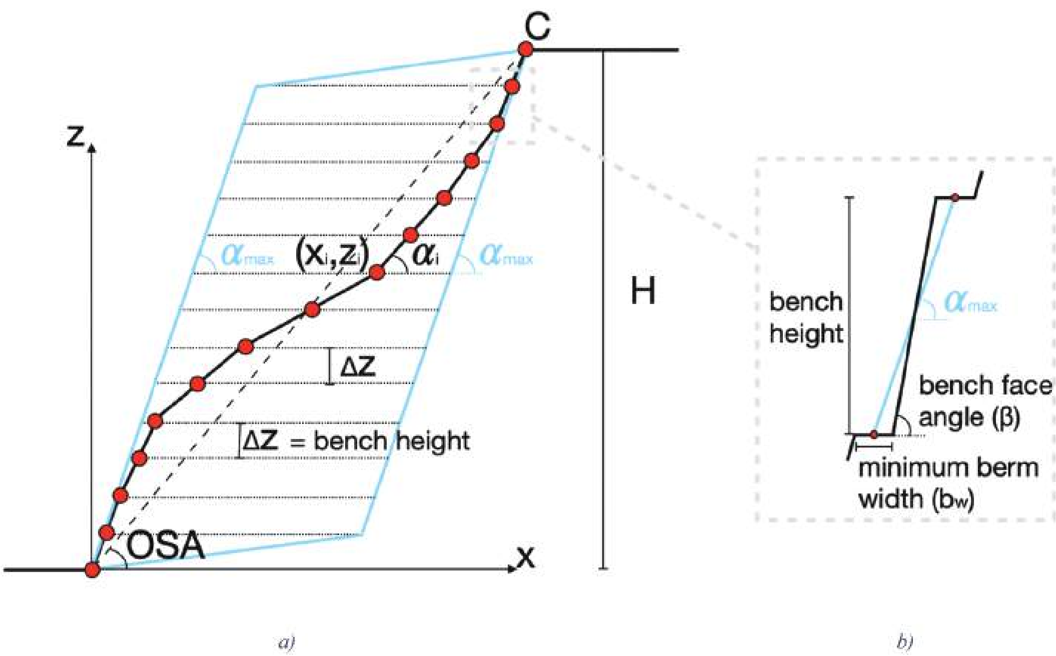

Figure 13. (a) A generic candidate slope profile. The toe of the profile is at the origin of the axes (x_0, y_0) and point C is the slope crest. A uniform discretization along the z direction is adopted. The blue lines enclose the region where the profiles are sought. The profile is discretised in n δz intervals so there are *n*-1 unknowns to be determined: x_1, x_2, … x_{n-1}. In the context of open pit mines, a good choice of Δz is to assume Δz equal to the bench height. b) determination of α_{imax} based on bench geometry.

algorithm is called on the basis of bench height, bench face inclination, and minimum berm width provided by the user (see Figure 13b). If a ramp needs to be included as part of the pitwall profile, a lower α_{imax} value is imposed for the profile segment corresponding to the vertical position of the ramp.

The optimal pitwall profile is defined as the overall steepest safe profile that meets the FoS design criterion (*i.e.*, OSA=OSA_{max}), with OSA being the inclination over the horizontal of the line joining the pitwall toe to the crest (see Figure 13). The logical steps used to calculate the optimal pitwall profile are summarised in Figure 14. Firstly, an initial OSA is heuristically determined using a database of stability charts derived from Hoek & Bray [5] based on some equivalent geomaterial geotechnical properties and the specified FoS. The main algorithm then calculates the optimal pitwall shape for the assigned OSA and geometric constraints (bench height, bench face inclination, minimum berm width, and road width). The FoS_i associated with the optimal profile found at the i-th iteration is then compared to the target FoS_{target}. If it is higher, a steeper OSA is prescribed at the next iteration; if it is lower, a flatter OSA is

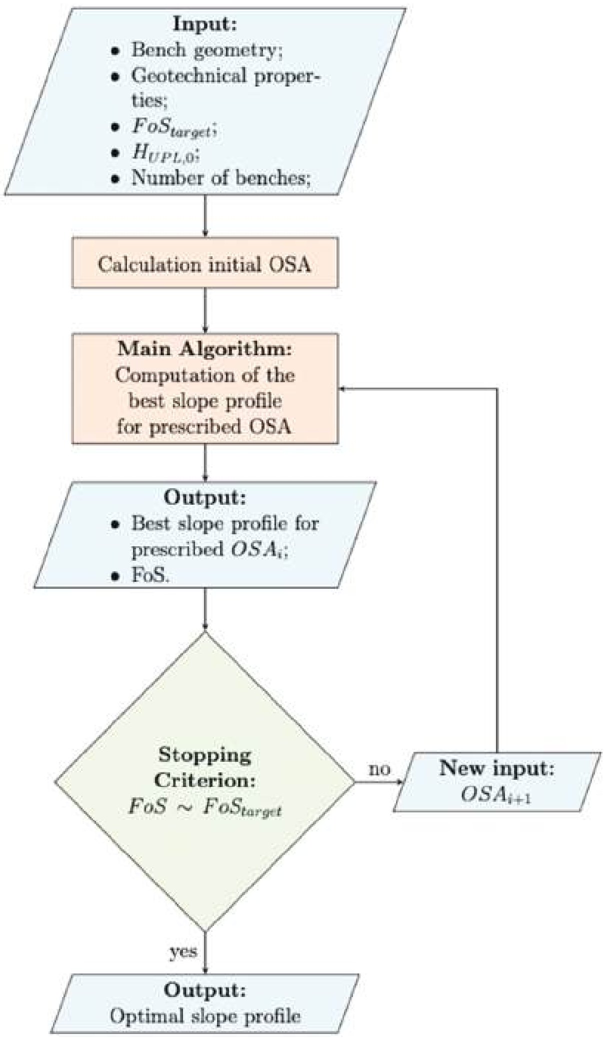

Figure 14. Flow chart summarizing the iterative procedure used to determine the optimal profile for a given pitwall after [13].

prescribed. The termination criterion is specified in terms of the percentage difference between FoS_{target} and FoS_i.

6. Results and discussion

Seven inclinations of bedding dip (0; 15; 30; 45; 60; 75; 90) were considered in order to fully investigate the effect of bedding dip inclination on slope topological optimisation (often in a mine the bedding in vertical cross-sections dips at different inclinations) together with three dip directions (hanging wall, footwall and side walls) for a total of 21 cross sections. Each cross section is characterised by different c - failure surface apparent dip and φ - failure surface apparent dip relationships and therefore by a unique anisotropic strength function. For each cross section, we designed two slope profiles: a planar one by trial and error (for every inclination considered, Rocscience Slide2 was employed to determine the FoS until convergence to the target value was achieved) and an optimal one calculated by OptimalSlope that satisfies the same FoS design criterion. A sensitivity analysis was conducted in Slide2 to check the independence of the calculated FoS from the number of slices adopted, resulting in a final number of slices equal to 200.

The obtained slope profiles are plotted in Figures 15a–g with each figure provided for a different value of bedding dip (i.e. Figure 15a for bedding dip 0 degrees, Figure 15b for bedding dip 15 degrees, etc). For each cross-section considered, the c - failure surface apparent dip and φ - failure surface apparent dip relationships are plotted in an inset in dark green and light green respectively; the profile found by OptimalSlope is plotted above, while the planar counterpart is plotted below. Each slope profile is plotted together with their FoS value, their failure surface which often includes a tension crack (red curve), and line of thrust (blue curve) determined by Slide2. Regarding the geometry of the failure mechanisms, it can be observed that they daylight at the slope toe in all the planar profiles whereas this is not always true for the optimal profiles.

In the former case, the result is to be expected from theory since slope failure is driven by the slope self-weight (no surcharge loads are present here), so the geometrical symmetry of planar

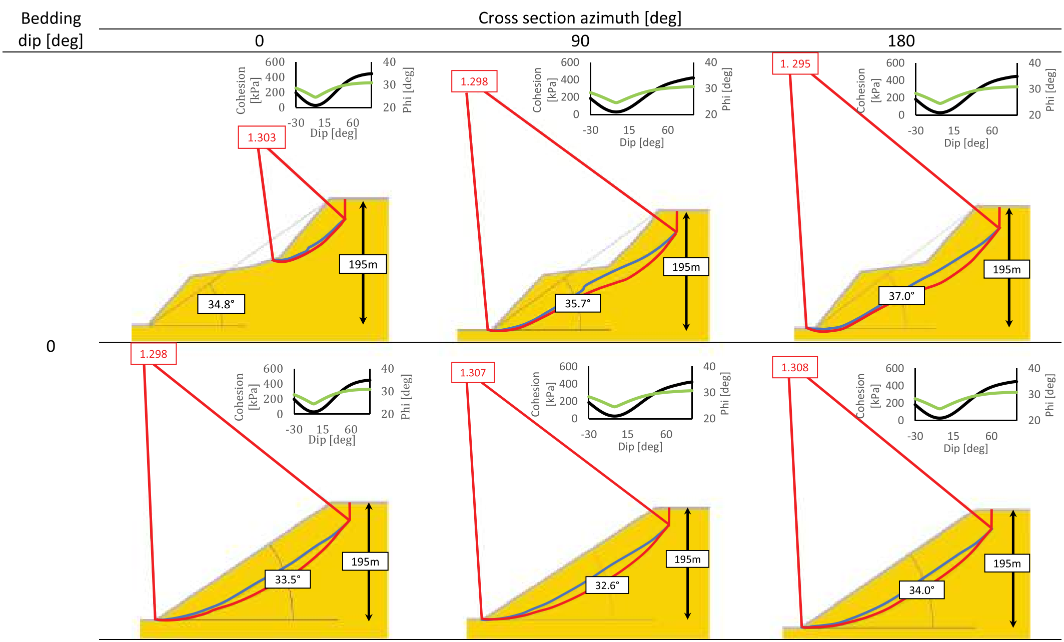

Figure 15a. Bedding dip 0 degrees; top row optimal profiles, and bottom row planar profiles for different cross section azimuths. The critical failure mechanism is displayed in red. The line of thrust is displayed in blue. The graph on the top right of each figure shows the functional relationship between (c, φ) and the apparent dip of the failure surface.

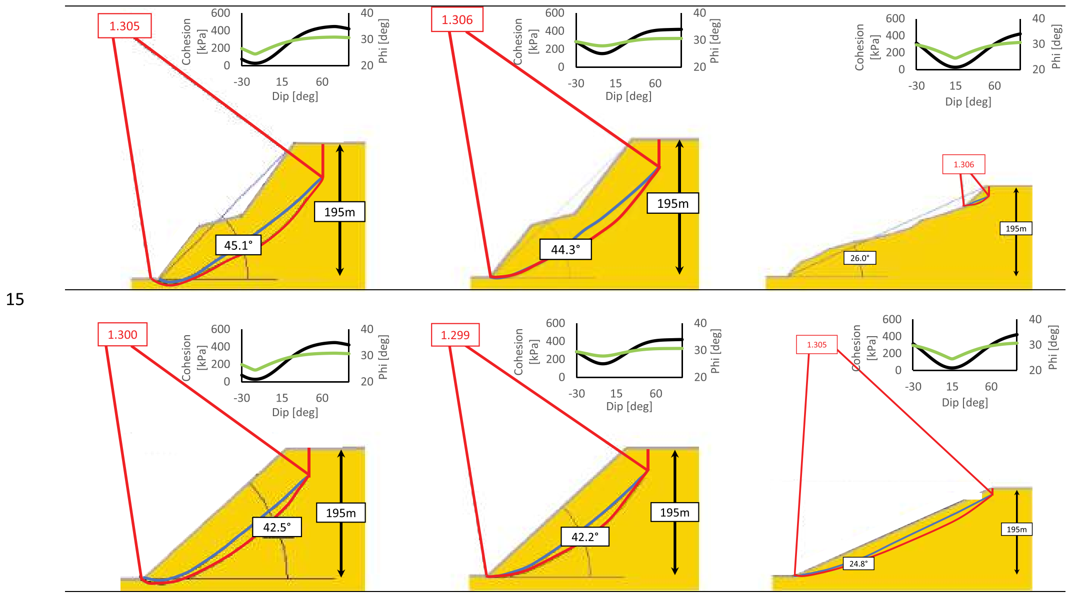

Figure 15b. Bedding dip 15 degrees; top row optimal profiles, and bottom row planar profiles for different cross section azimuths. The critical failure mechanism is displayed in red. The line of thrust is displayed in blue. The graph on the top right of each figure shows the functional relationship between (c, φ) and the apparent dip of the failure surface.

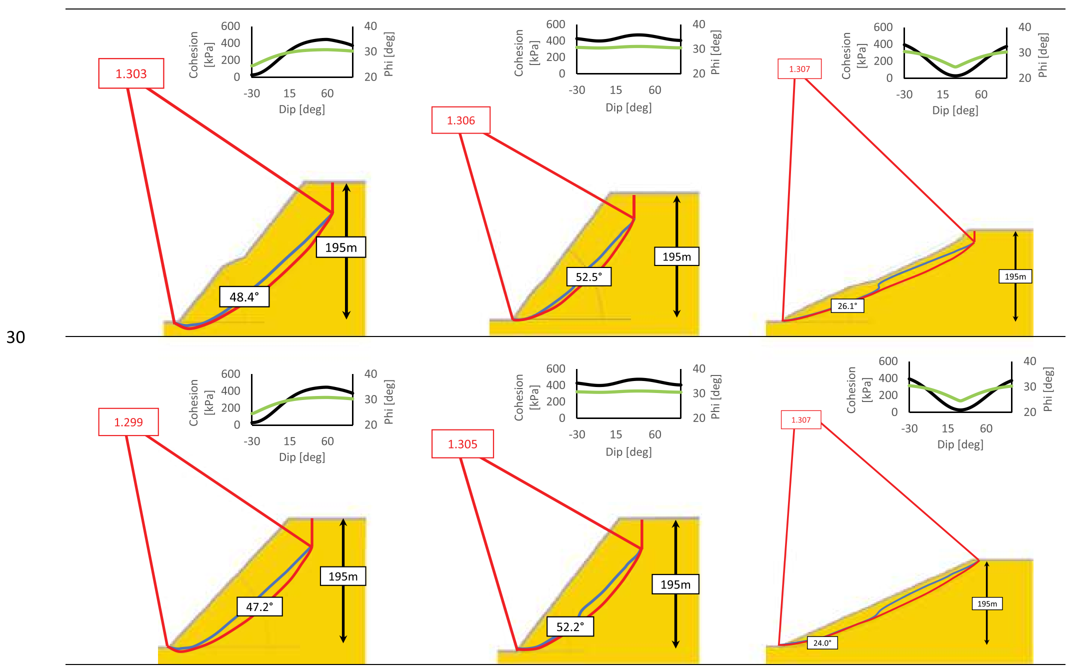

Figure 15c. Bedding dip 30 degrees; top row optimal profiles, and bottom row planar profiles for different cross section azimuths. The critical failure mechanism is displayed in red. The line of thrust is displayed in blue. The graph on the top right of each figure shows the functional relationship between (c, φ) and the apparent dip of the failure surface.

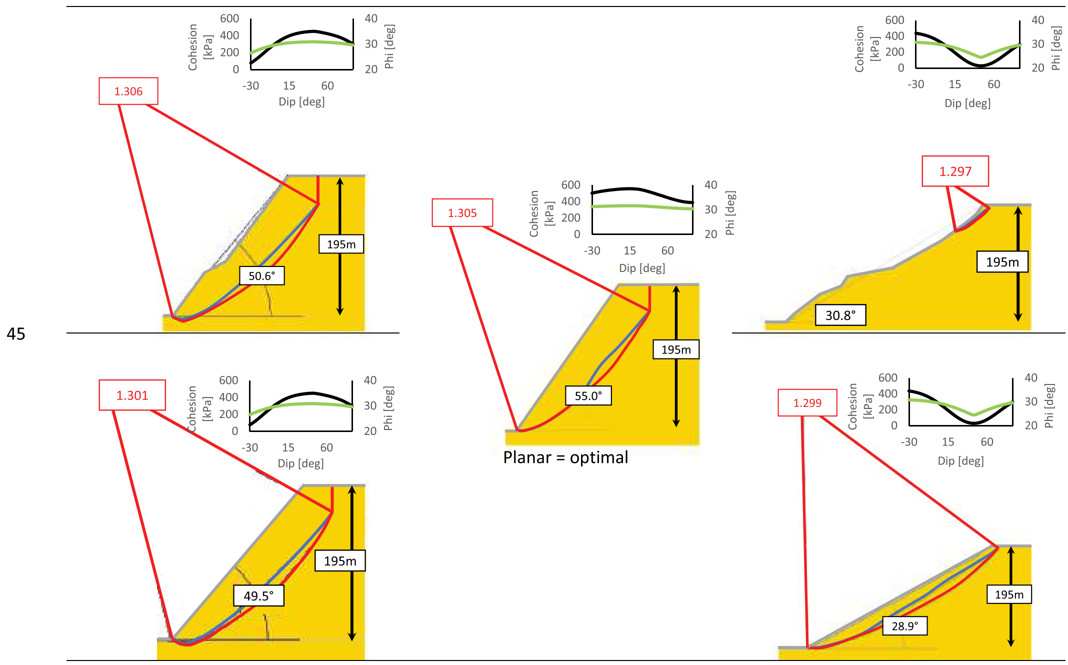

Figure 15d. Bedding dip 45 degrees; top row optimal profiles, and bottom row planar profiles for different cross section azimuths. The critical failure mechanism is displayed in red. The line of thrust is displayed in blue. The graph on the top right of each figure shows the functional relationship between (c, φ) and the apparent dip of the failure surface.

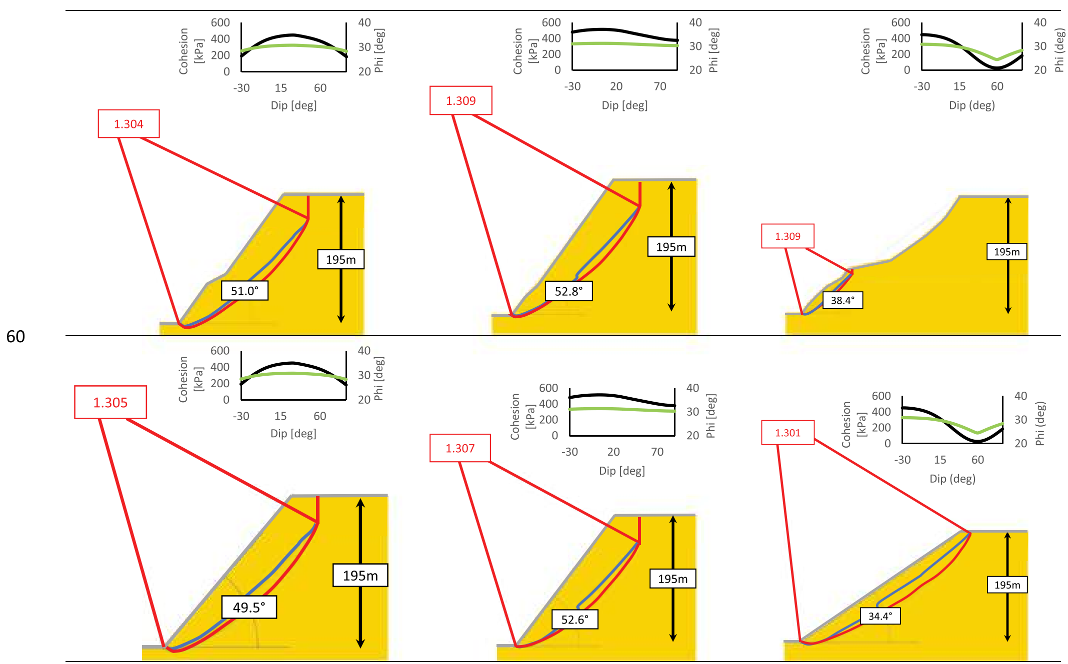

Figure 15e. Bedding dip 60 degrees; top row optimal profiles, and bottom row planar profiles for different cross section azimuths. The critical failure mechanism is displayed in red. The line of thrust is displayed in blue. The graph on the top right of each figure shows the functional relationship between (c, φ) and the apparent dip of the failure surface.

75

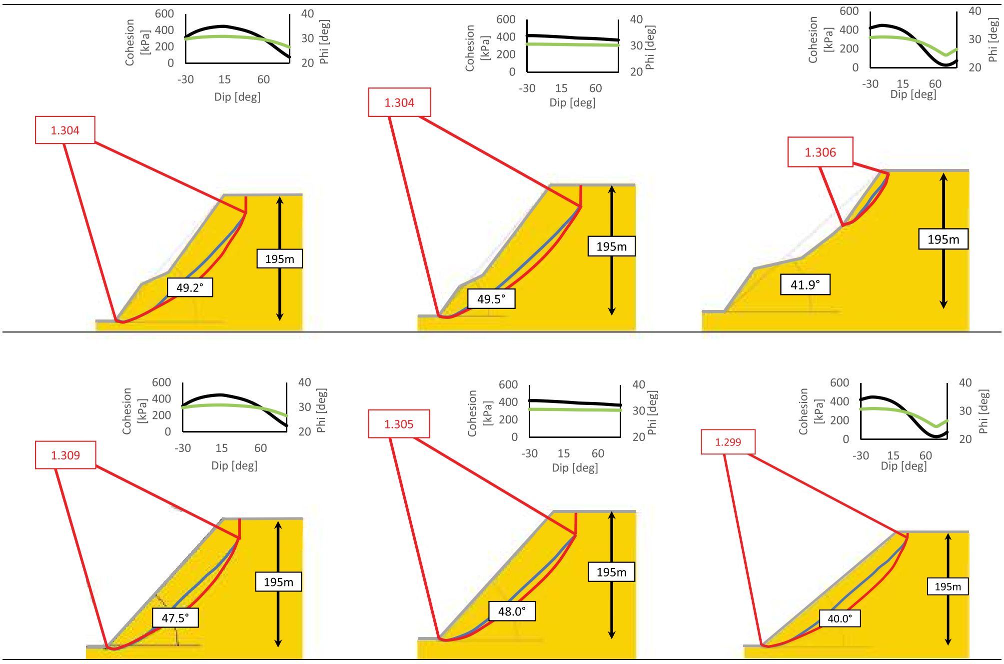

Figure 15f. Bedding dip 75 degrees; top row optimal profiles, and bottom row planar profiles for different cross section azimuths. The critical failure mechanism is displayed in red. The line of thrust is displayed in blue. The graph on the top right of each figure shows the functional relationship between (c, φ) and the apparent dip of the failure surface.

90

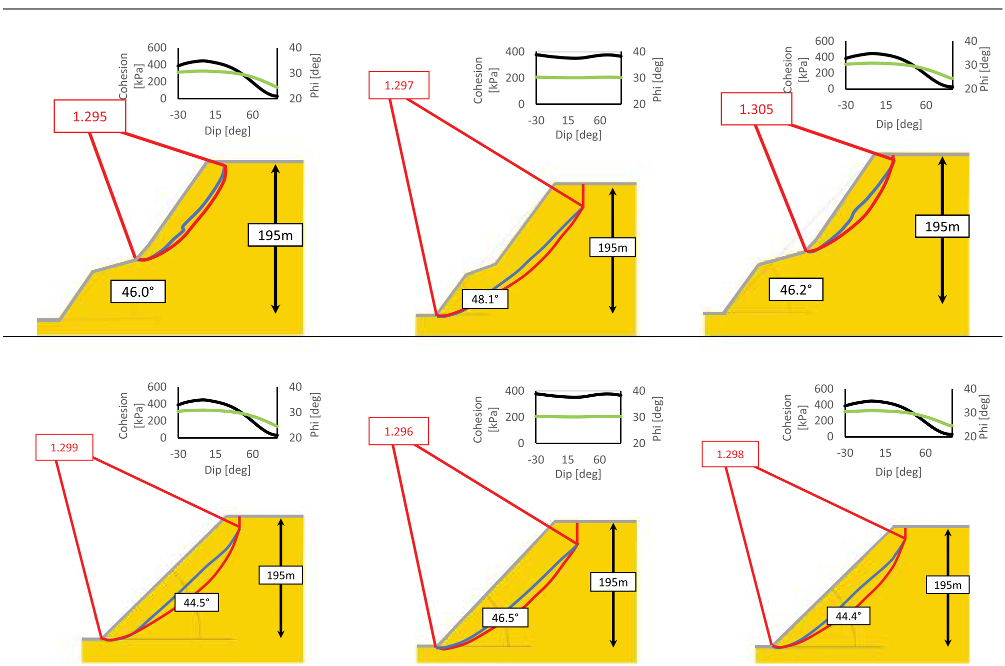

Figure 15g. Bedding dip 90 degrees; top row optimal profiles, and bottom row planar profiles for different cross section azimuths. The critical failure mechanism is displayed in red. The line of thrust is displayed in blue. The graph on the top right of each figure shows the functional relationship between (c, φ) and the apparent dip of the failure surface.

profiles dictates that in the absence of discrete geological discontinuities (e.g. a fault or rock layer contact surfaces) for uniform (c, φ) slopes, it has to be expected that the failure mechanism daylights at the slope toe or below since the deeper the mechanism, the more critical it is. However, the mechanism could daylight below the toe as well, but this only happens for $\varphi < 5$ [33,43]. While the friction angle of the slopes considered here varies depending on the loading shearing direction, the average value in the range of shearing directions of interest is always > 5. Note that in principle the presence of tension cracks could cause the failure mechanism to daylight on the slope face, but Utili [45] has shown this never to be the case for isotropic slopes.

Regarding the optimal slope profiles, the failure mechanism does daylight above the profile toe in a few cases (Figures 15a, 15b, 15d–15g). First, it is observed that unlike planar slope profiles, optimal profiles are highly non-linear and therefore it is perfectly possible the failure surface daylights above the toe. Second, LEM analyses show that in the case of optimal profiles, there are several competing failure mechanisms with factor of safety values very close to each other. From the theory of elasto-perfect plasticity (the constitutive model assumed in limit analysis), we know that the larger the volume of a solid undergoing yield before collapsing, the higher is its resistance to collapse (a typical example in structural engineering is the higher the number of plastic hinges developing in a building before collapse, the better). The presence of several competing failure mechanisms, i.e. featured by similar FoS values, points to a large area of the slope being at yield before collapse is reached. These observations point to a fundamental physical property of the optimal profiles, which is they maximise slope resistance to failure by shaping the slope profile such that the extent of the slope region where the ground strength is fully mobilised is maximised.

In Figure 16, all the optimal slope profiles are plotted, grouped by the direction of the cross-section azimuth. The optimal profiles with cross-section azimuth of 90/270 degrees (end wall) tend to approach the planar profiles with an inclination equal to the maximum

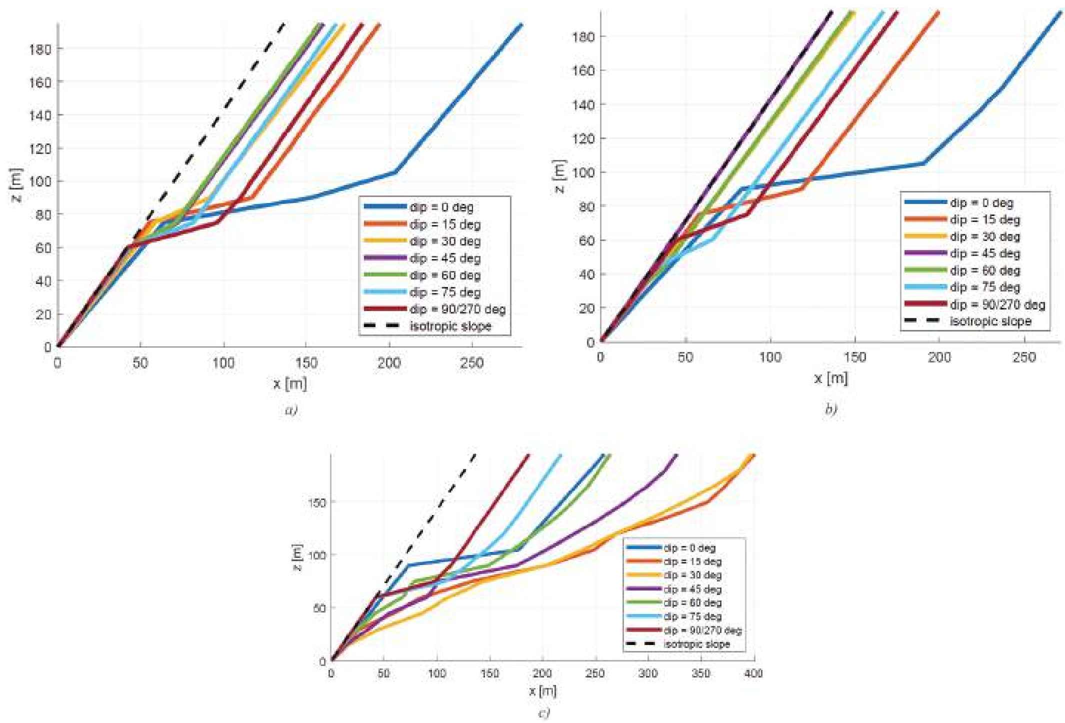

Figure 16. Optimal slope profiles grouped according to different cross section azimuth: a) hanging wall (ddr = 0 deg); b) end wall ddr = 90/270 deg); c) footwall (ddr = 180 deg).

interramp angle (55 degrees) controlled by bench design; this is because anisotropy has the least impact on the end walls. On the other hand, optimal profiles characterised by cross-section azimuth equal to 180 degrees (footwall) are flatter, and where the optimal slope profiles perform best and can consistently achieve a steeper OSA for the same FoS criterion. In general, the geotechnically optimal profiles are featured by steeper slope segments near the crests and toes of the slopes, with a flatter segment at approximately one-third of the total height of the slope.

To investigate the influence of anisotropy on the shape of optimal profiles, we have determined both the planar and the optimal shape for a reference isotropic pitwall with the isotropic strength parameters obtained by calculating the equivalent continuum Generalised Hoek Brown parameters. These parameters were obtained from compression test laboratory data (UCS = 47.3 MPa, m_i = 16.9) and empirical observations (GSI = 30). Regarding the parameter D (disturbance factor), which accounts for weakening of rock strength due to excavation induced stress relaxation and blasting, its determination is more uncertain with published values sometimes varying widely. Recently, Yang et al. [52] have carried out experimental measurements of hardness in an open pit mine showing that in case of well controlled blasting, only a few metres of rock are disturbed. This would point to using D = 0 in the slope, however here the excavation is deeper than the slopes considered by Yang et al. [52]. Also, in current practice, most pitwall designers employ some value of D to account for stress relaxation effects. Albeit D varies within a slope, here instead we assumed a uniform D for sake of simplicity. We ran analyses for three scenarios: D = 0 (optimistic), D = 0.15 (medium), and D = 0.30 (conservative). In all of them, the optimal shape for the isotropic case (see dashed line in Figure 16) is planar due to the constraint exerted by bench geometry (see Section 4.4 and Section 5), which limits the inter-ramp maximum inclination to 55 degrees. In this case, slope design is bench controlled and the optimal profile coincides with the planar one. Comparing the optimal profile shapes obtained for the isotropic case with the shapes obtained for the anisotropic cases shows unequivocally the large influence of anisotropy on the optimal profile shapes. This means that neglecting anisotropy would lead to either very suboptimal results (in cases where the anisotropic strength is larger than the isotropic one) or unsafe (in cases where the anisotropic strength is smaller than the isotropic one).

Figure 17 reports a graphical comparison between the OSA of the planar pitwall profiles and of the optimal pitwall profiles. Overall, the optimal profile is steeper than the planar profile up to 3.1 degrees. However, for the pitwall profiles with bedding dip equal to 30, 45, and 60 degrees and cross section azimuth equal to 90/270 degrees, the improvement in OSA of the optimal profile over the planar one is almost negligible because the relationships between (c, φ) and dip of the failure surface (see central column of Figures 15c–e) allow for an OSA almost equivalent to the maximum interramp angle. For the cross section with bedding dip of 45 degrees and azimuth 90 degrees, only a planar slope profile is obtained (see Figure 15d) since the bench face inclination and minimum berm width limit the maximum OSA of the pitwall to the value of the inter-ramp angle (i.e. 55 degrees), resulting in a FoS equal to the minimum acceptable value of 1.3. Hence because the geometry of the benches entirely dictates the OSA of the profile, the profile cannot be improved by the slope optimiser, so the pitwall profiles adopted in this cross section for both types of design are the same.

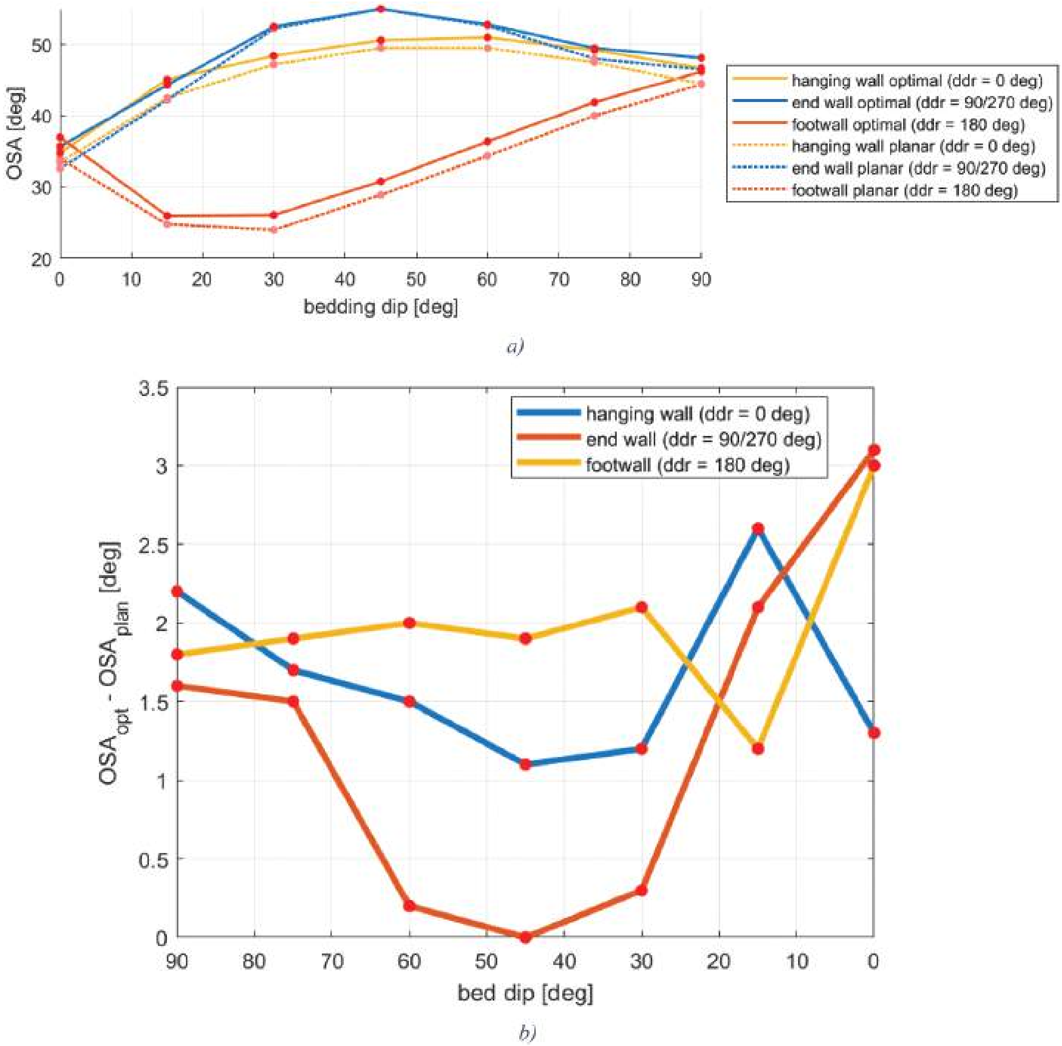

Figure 17. Overall Slope Angles (OSA) calculated for all the cross sections analysed, with each cross section indicated by a full circle: a) bedding dip vs OSA for the optimal and planar pitwall profiles ; b) bedding dip vs OSA increment achieved by the adoption of optimal profiles (calculated as OSA of the optimal profile minus OSA of the planar counterpart).

7. Conclusions

A new methodology for topological optimisation of anisotropic slopes is presented to determine geotechnically optimal profiles – profiles that maximise the overall slope angle for a prescribed FoS, considering the geometry of benches and any ramps – for rock masses featuring multiple joint sets in 3D. The methodology presented is versatile, allowing implementation of any anisotropy function with varying levels of discretisation.

A discontinuity data set from a Cretaceous-aged siltstone with eight different joint sets and one main bedding set was analysed. Optimal slope profiles were determined for various bedding dips (0, 15, 30, 45, 60, 75, 90) and pitwall orientations (footwall, hanging wall, and side wall), covering a wide range of excavation scenarios, thereby providing a realistic sensitivity analysis of the potential gain in overall slope angle achievable for a bedded sedimentary rock.

The simulations results show that optimal pitwall profiles can significantly increase the overall slope angle up to 3 degrees in comparison with planar profiles featured by the same FoS. LEM stability analyses of all the optimal profiles calculated by OptimalSlope were performed using Rocscience Slide 2 to independently verify the FoS and failure mechanism of the profiles obtained. In all cases, the FoS determined by OptimalSlope closely matched the target value of 1.3, with the geometry of the failure mechanism also being closely matched. This confirms that the optimal pitwall profiles are as safe as their planar counterparts.

The reported improvements in pitwall inclinations (all above 1 degree except in three cases of anisotropy) are substantial and comparable in magnitude to those reported in other mine case studies where optimal slope profiles were determined by OptimalSlope for isotropic rock masses [11–13]. In those mine case studies, the adoption of optimal pitwall profiles resulted in Net Present Value improvements ranging from 12 to 140 millions of USD, along with significant reductions in carbon footprint due to reduced excavated waste rock.

Lastly, this study highlights the importance of accounting for rock mass strength anisotropy. In fact the optimal profiles calculated for isotropic rock strength parameters, derived from equivalent continuum Generalised Hoek Brown parameters, are geometrically distinct from the profiles determined accounting for the rock mass anisotropic strength [53].

Notations

b_w	bench width
H_{bench}	bench height
γ	unit weight of the geomaterial
H	height of the overall slope
c_{rm}	cohesion of the rock mass
α_{fail}	average inclination of each piecewise segments of the failure surface
i	numbering of the piecewise segments making the failure surface
Ω	angular velocity of the failing mass
V	tangential velocity of the failing mass
θ and r	polar coordinates, with respect to the centre of instantaneous rotation (O), of the piecewise segments dividing the failure surface
r_0	length of the chord OB
c_i	cohesion of each piecewise segmentof the failure surface
φ_i	angle of internal friction for each piecewise segment of the failure surface
W_d	rate of dissipated energy along the failure surface
W_E	rate of work done by the failing mass

Disclosure statement

No potential conflict of interest was reported by the author(s).

ORCID

Stefano Utili http://orcid.org/0000-0003-3156-8013

References

[1] M. Randolph, *Current Trends in Mining. SME Mining Engineering Handbook*, 3rd ed. Society for Mining Metallurgy & Exploration, 2011, pp. 11–21.
[2] W. Hustrulid, M. Kuchta, and R. Martin, *Open Pit Mine Planning & Design*, CRC Press, Boca Raton, Florida, 2013; London: Taylor & Francis distributor.
[3] E.T. Brown, *Geomechanics: The critical engineering discipline for mass mining*, in *Massmin 2004*, A. Karzulovic and M. Alfaro, eds. Chilean Engineering Institute, Santiago, Chile, 2004, pp. 21–36.
[4] J. Newman, *Earthwork Slips and Subsidences Upon Public Works*, E. & F. N. Spon, London, 1890.
[5] E. Hoek and J. Bray, *Rock Slope Engineering*, The Institution of Mining and Metallurgy, London, 1977.
[6] S. Utili and R. Nova, *On the optimal profile of a slope*, Soils Found. 47 (4) (2007), pp. 717–729. doi:10.3208/sandf.47.717.

[7] I.A. Jeldes, E.C. Drumm, and D.C. Yoder, *Design of stable concave slopes for reduced sediment delivery*, J. Geotech. Geoenviron. Eng. 141 (2) (2015), doi:10.1061/(ASCE)GT.1943-5606.0001211.

[8] F. Vahedifard, S. Shahrokhabadi, and D. Leshchinsky, *Optimal profile for concave slopes under static and seismic conditions*, Can. Geotech. J. 53 (9) (2016), pp. 1522–1532. doi:10.1139/cgj-2016-0057.

[9] T. Vo and A.R. Russell, *Stability charts for curvilinear slopes in unsaturated soils*, Soils Found. 57 (4) (2017), pp. 543–556. doi:10.1016/j.sandf.2017.06.005.

[10] S. Utili, OptimalSlope: Software for the determination of optimal profiles for slopes and pitwalls, 2016.

[11] A. Agosti, S. Utili, D. Gregory, A. Lapworth, J. Samardzic, and A. Prawasono, *Design of an open-pit gold mine by optimal pitwall profiles*, CIM J. 11 (4) (2021), pp. 149–168. doi:10.1080/19236026.2021.1979382.

[12] A. Agosti, S. Utili, C. Valderrama, and G. Albornoz, *Optimal pitwall profiles to maximise the overall slope angle of open pit mines: The McLaughlin Mine*, in *SSIM 2021: Second Int Slope Stability in Mining, Australian Centre for Geomechanics*, P. Dight, ed. 2021, pp. 69–82. doi:10.36487/ACG_repo/2135_01.

[13] S. Utili, A. Agosti, N. Morales, C. Valderrama, R. Pell, and G. Albornoz, *Optimal pitwall shapes to increase financial return and decrease carbon footprint of open pit mines*, Min. Metall. Explorat. 39 (2022), pp. 335–355. doi:10.1007/s42461-022-00546-8.

[14] A. Agosti, S. Utili, J. Tasker, C. Zhao, P. Knights, M. Nerhing, and S. Zia, *The effect of carbon tax and optimal profiles on profitability and emissions of open pit mines*, Min. Technol. 132 (1) (2023), pp. 1–16. doi:10.1080/25726668.2022.2122336.

[15] N. Bar and G. Weekes, *Directional shear strength models in 2D and 3D limit equilibrium analyses to assess the stability of anisotropic rock slopes in the Pilbara region of Western Australia*, Aus. Geomech. 52 (2017), pp. 91–104.

[16] M. Bester, T.R. Stacey, and T. Russell, *Synthetic rock mass modelling and geotechnical mapping: An open pit mine case study in anisotropic rock*, Int. J. Min. Reclam. Environ. 35 (5) (2020), pp. 356–378. doi:10.1080/17480930.2020.1834177.

[17] G.J.C. Gomes, J.H. Forero, E.A. Vargas, and J.A. Vrugt, *Bayesian inference of rock strength anisotropy: Uncertainty analysis of the hoek–brown failure criterion*, Int. J. Rock Mech. Min. Sci. 148 (2021), pp. 1004952. doi:10.1016/j.ijrmms.2021.104952.

[18] J. Liu, S. Sun, L. Yue, J. Wei, and J. Wu, *Mechanical and failure characteristics of rock-like material with multiple crossed joint sets under uniaxial compression*, Adv. Mech. Eng. 9 (7) (2017), pp. 1–18. doi:10.1177/1687814017708710.

[19] K. Mercer, The history and development of the anisotropic linear model: Part 1, *Australian Centre for Geomechanics*, 2012, July Newspaper.

[20] K.G. Mercer, The history and development of the anisotropic linear Model: Part 2, Australian Centre for Geomechanics, 2013, pp. 17, July Newspaper 2013.

[21] K. Mercer, *Ongoing research into anisotropic rock masses using numerical modelling*, in *Australian Centre for Geomechanics*, P. Dight, ed., 2013, Australian Centre for Geomechanics, Perth. pp. 237–247.

[22] B. Sainsbury, M. Pierce, and D. Mas Ivars, *Simulation of rock mass strength anisotropy and scale effects using a ubiquitous joint rock mass (UJRM) model*, in *Continuum and Distinct Element Numerical Modeling in Geo-Engineering - 2008*, R.D. Hart and C. Detournay, eds., Itasca Consulting Group, Inc., Minneapolis, 2008. Paper: 06–02.

[23] D. Sainsbury and B.A. Sainsbury, *Three-dimensional analysis of pit slope stability in anisotropic rock masses*, Proceedings of the 2013 International Symposium on Slope Stability in Open Pit Mining and Civil Engineering, Australian Centre for Geomechanics, Perth, 2013, pp. 683–695. doi:10.36487/ACG_rep/1308_45_Sainsbury.

[24] J.M. Seery, *Limit equilibrium analysis of a planar sliding example in the Pilbara region of Western Australia – comparison of modelling discrete structure to three anisotropic shear strength models*, Slope Stab. (2015), pp. 18.

[25] P. Wang, F. Ren, S. Miao, M. Cai, and T. Yang, *Evaluation of the anisotropy and directionality of a jointed rock mass under numerical direct shear tests*, Eng. Geol 225 (2017), pp. 29–41. doi:10.1016/j.enggeo.2017.03.004.

[26] D. Martin and P. Stacey, *Guidelines for Open Pit Slope Design in Weak Rocks*, CSIRO Publishing, Clayton, Vic, 2018.

[27] J. Read and P. Stacey, *Guidelines for Open Pit Slope Design*, CSIRO Pub, Collingwood, Victoria, 2009.

[28] S.D. Cylwik, *Three-Dimensional Anisotropic Shear Strength of Jointed Rock Masses*, ARMA, Houston, Texas, USA, 2021.

[29] D.M. Ivars, M. Pierce, D. DeGagné, and C. Darcel, *Anisotropy and scale dependency in jointed rock-mass strength – a synthetic rock mass study*, in *Continuum and Distinct Element Numerical Modeling in Geo-Engineering - 2008*, R.D. Hart and C. Detournay, eds., Itasca Consulting Group, Inc., Minneapolis, 2008. Paper: 06–01.

[30] M. Board, E. Chacon, P. Varona, and L. Lorig, *Comparative analysis of toppling behaviour at chuquicamata open-pit mine, Chile*, Trans. Inst. Min. Metall. Sect. A Min. Ind. 105 (1996), pp. A11–A21.

[31] B.L. Sainsbury and D.P. Sainsbury, *Practical use of the ubiquitous-joint constitutive Model for the simulation of anisotropic rock masses*, Rock Mech. Rock Eng. 50 (6) (2017), pp. 1507–1528. doi:10.1007/s00603-017-1177-3.

[32] K.Y. Lo, *Stability of slopes in anisotropic soils*, J. Soil Mech. Found. Div. 91 (4) (1965), pp. 85–106. doi:10.1061/JSFEAQ.0000778.
[33] W.F. Chen, *Limit Analysis and Soil Plasticity*, Elsevier Scientific Pub. Co, Amsterdam; Oxford; New York, 1975.
[34] E. Stockton, B.A. Leshchinsky, M.J. Olsen, and T.M. Evans, *Influence of both anisotropic friction and cohesion on the formation of tension cracks and stability of slopes*, Eng. Geol. 249 (2019), pp. 31–44. doi:10.1016/j.enggeo.2018.12.016.
[35] E. Hoek and E.T. Brown, *Empirical strength criterion for rock masses*, J. Geotech. Engrg. Div. 106 (GT9) (1980), pp. 1013–1035. doi:10.1061/AJGEB6.0001029.
[36] E. Hoek, C. Carranza-Torres, and B. Corkum, *Hoek-Brown failure criterion – 2002 edition*, Proc NARMS-TAC Conference, Toronto, 2002, pp. 267–273.
[37] K. Colak and T. Unlu, *Effect of transverse anisotropy on the hoek–brown strength parameter 'mi' for intact rocks*, Int. J. Rock Mech. Min. Sci. 41 (6) (2004), pp. 1045–1052. doi:10.1016/j.ijrmms.2004.04.004.
[38] M.A. Ismael, H.F. Imam, and Y. El-Shayeb, *A simplified approach to directly consider intact rock anisotropy in hoek–brown failure criterion*, J. Rock Mech. Geotechnical. Eng. 6 (5) (2014), pp. 486–492. doi:10.1016/j.jrmge.2014.06.003.
[39] H. Saroglu and G. Tsiambaos, *A modified Hoek–brown failure criterion for anisotropic intact rock*, Int.J. Rock Mech. Min. Sci. 45 (2) (2007), pp. 223–234. doi:10.1016/j.ijrmms.2007.05.004.
[40] J.C. Jaeger, *Shear failure of anisotropic rocks*, Geol. Mag. 97 (1) (1960), pp. 65–72. doi:10.1017/S0016756800061100.
[41] N. Bar, T. Johnson, and G. Weekes, *Using directional shear stress models to predict slope stability in highly anisotropic rock masses*, in *Rock Mechanics and Rock Engineering*: From the Past to the Future, CRC Press, Cappadocia, Turkey, 2016, pp. 595–600. doi:10.1201/9781315388502-103.
[42] T.M. Ryan, Shear strength of closely jointed porphyry rock masses, Alaska rocks 2005, 40th US symposium on rock mechanics (ARMA), 2005.
[43] D.W. Taylor, *Stability of earth slopes*, J. Boston Soc. Civ. Eng. 24 (1937), pp. 197–247.
[44] R.L. Michalowski, *Slope stability analysis: A kinematical approach*, Géotechnique 45 (2) (1995), pp. 283–293. doi:10.1680/geot.1995.45.2.283.
[45] S. Utili, *Investigation by limit analysis on the stability of slopes with cracks*, Géotechnique 63 (2) (2013), pp. 140–154. doi:10.1680/geot.11.P.068.
[46] D.E. Nicholas and D.B. Sims, *Collecting and using geologic structure data for slope design*, in *Slope Stability in Surface Mining*, W. Hustrulid, McCarter, M.K, Van Zyl, D.J.A., eds., Society for Mining, Metallurgy, and Exploration, Littleton, Colorado, 2001. pp. 11–26.
[47] S.D. Cylwik, 3D/2D anisotropic strength estimation worksheet, 2022.
[48] P. Darling, *SME Mining Engineering Handbook*. SME, editors. 3rd. ed. SME - Soc. for Mining, Metallurgy, and Exploration, Englewood, Col, 2011.
[49] H.L. Hartman, S.G. Britton, D.W. Gentry, M. Karmis, J.M. Mutmansky, and W.J. Schlitt, *SME Mining Engineering Handbook*, 2nd ed. Society for Mining, Metallurgy, and Exploration, Littleton, Colorado, 1992.
[50] T.M. Ryan and P.R. Pryor, *Designing catch benches and interramp slopes*, in *Slope Stability in Surface Mining, SME - Soc. for Mining, Metallurgy, and Exploration*, W.A. Hustrulid, M.K. McCarter, and D.J.A. Van Zyl., eds., Society for Mining, Metallurgy, and Exploration, Littleton, Colorado, 2001. pp. 27–38.
[51] N. Morgenstern and V.E. Price, *The analysis of the stability of general slip surfaces*, Géotechnique 15 (1) (1965), pp. 79–93. doi:10.1680/geot.1965.15.1.79.
[52] J. Yang, J. Dai, C. Yao, S. Jiang, C. Zhou, and Q. Jiang, *Estimation of rock mass properties in excavation damage zones of rock slopes based on the hoek-brown criterion and acoustic testing*, Int. J. Rock Mech. Min. Sci. 126 (2020), pp. 104192. doi:10.1016/j.ijrmms.2019.104192.
[53] R.D. Call, *Slope stability*, in *ME Mining Engineering Handbook*, H. Hartman, ed. 2nd ed., vol 1, SME, Littleton, Colorado, 1992. pp. 495–526.